energies

MDPI

Article

Voltage Quality Enhancement of Grid-Integrated PV System Using Battery-Based Dynamic Voltage Restorer

Emiyamrew Minaye Molla and Cheng-Chien Kuo *

Department of Electrical Engineering, National Taiwan University of Science and Technology, 43, Sec. 4, Keelung Rd., Da'an District, Taipei City 10607, Taiwan; minaye.emiyamrew@yahoo.com

* Correspondence: cckuo@mail.ntust.edu.tw; Tel.: +886-920-881-490; Fax: +886-227-376-688

Received: 10 October 2020; Accepted: 30 October 2020; Published: 2 November 2020

Abstract: The advancement of power electronic-based sensitive loads drives the power utilities' devotion to power quality issues. The voltage disturbance could be happening due to fault conditions, switching of loads, energizing of transformers, or integration of highly intermittent energy sources such as PV systems. This research work attempts to enhance the voltage fluctuation of a sensitive load connected to a grid-integrated PV system using a battery-based dynamic voltage restorer (DVR). The proposed battery energy storage-based DVR has two separate controlling stages that are implemented at the DC–DC buck/boost converter of the battery and voltage source converter (VSC) system. Charging and discharging of the battery is operated based on the state-of-charge (SOC) value of the battery and the measured root mean square (RMS) voltage at the point of common coupling (PCC). The VSC of the DVR detection and reference generation control is done appropriately. In the detection control of the VSC, a combination of RMS and dq0 measurement techniques is used, whereas in the reference generation control, pre-fault strategy is implemented to restore both phase jump and magnitude distortions. Symmetrical and asymmetrical voltage sags scenarios are considered and the compensation demonstration is carried out using power system computer-aided design (PSCAD/EMTDC) software.

Keywords: converters; dynamic voltage restorer (DVR); photovoltaic systems; power distribution faults; power filters; state of charge (SOC)

1. Introduction

Exploitation of nonrenewable energy sources threatens our planet with extreme exposure to global warming and climate change. Due to this, for the past few years and nowadays, leaders and policy makers overlay utilization of renewable energy sources (RES) with wind and solar photovoltaic (PV) power standing out in particular [1]. Based on the past trends, PV power is one of the fastest-growing technologies which gets vital emphasis and attracts both industries and customers in view of energy shortages and environmental concerns [1–4]. Especially, it has immensely evolved in the building energy sector for which it is predominantly relevant and this clearly appears through distributed grid-connected systems. The green energy policies and technological advancements play a vital role in helping PV expansion with progressive cost reduction. Expansion of grid-connected PV systems in various energy sectors is expected to continue in the next decade [5].

Even though RES are environmentally friendly and abundant in nature, their output power is not stable due to their source intermittent characteristics. The global trend of grid-connected PV power plant installation indicates a fast pace. The installation is expected to grow more by developing and applying additional regulations and standards to minimize the potential adverse impacts of large PV

power plants on the reliability and stability of the electricity network [6]. Due to this, in order to get firm power output, in most cases the installation of RES is implemented by integrating them with energy storage (ES) systems to mitigate this intermittency [1,7–9] and battery ES (BES) is commonly used for these RES [6]. Even though BES is commonly used, there are also numerous ES technologies available in the market, though all of them are still expensive for PV applications [1].

Power quality (PQ) is a vital issue, especially in commercial and industrial sectors, for delivering its clients a reliable and economical supply. As nonlinear electrical loads are used more frequently, the PQ impacts are increasing, which have great implications for industrial and domestic consumers [10,11]. PQ mainly depends upon the nature of the supply system and the type of loads connected in the distribution system [12]. The widespread use of advanced power electronic-based digital equipment, such as adjustable speed drives, computers, automated manufacturing industries, and so forth, increases the attention of the PQ in modern distribution systems. These devices will malfunction when vulnerable to voltage disturbances such as voltage sags, swells, flicker, harmonics, and momentary interruptions. PQ problems have measurable and immeasurable cost effects on both power providers and customers. Industrial customers' financial losses due to disruption or malfunction of equipment caused by voltage fluctuation could be substantial. The financial loss is also significant when the fluctuation happens in commercial customers such as banks, data centers, customer service centers, and so on [13].

In industrial distribution systems, the grid voltage disturbances are typically caused by symmetrical and unsymmetrical faults, energization of transformers, starting of large motors, switching of linear and nonlinear loads, capacitor banks, and integration of highly intermittent renewable sources like PV and wind [14,15]. Voltage sag is the most frequent voltage disturbance and always appears with a phase angle jump. The phase jump in the voltage will actuate transient current in the capacitors, transformers, and motors. It is therefore crucial to protect sensitive loads from being affected and damaged by voltage and current distortion [15]. The increased penetration of the RES to the utility grid poses intimidation to the PQ, load mismatch, frequency deviation, and insufficient load following [16]. So the drawbacks of RES should be improved to utilize effectively with the fast growth of its contribution to substitute the nonrenewable energy sources [12].

Different flexible AC transmission system (FACTS) devices such as a distribution static synchronous compensator (DSTATCOM), static VAR compensator (SVC), and DVR which are power electronic-based devices are used in AC transmission networks to increase power stability. This will be done by controlling network parameters (current, voltage, and impedance) effectively to mitigate voltage sag, swell, flicker, and harmonics through the series and/or shunt compensation [17]. These FACTS devices are widely applicable for on-grid RES output power smoothing which provides reactive power compensation, power factor correction, harmonics filtering, and mitigation of other power quality issues [18–21]. FACTS devices' voltage restoration capability is influenced by various factors, such as the power converter rating, the load to be serviced, the voltage sag/swell depth, and the properties of the power system at the load location [17].

DVR is the most comprehensive and cost-effective FACTS device which is connected in series at the distribution feeder. Nowadays, its application for wind and PV power systems has increased [20–24] which is competent for generating or absorbing real and reactive power at its AC terminals [25]. Grid-connected [26] and off-grid [20,27] wind power quality improvement research was done using a DVR without energy storage. But the DVRs used in these research works will not be that successful during deep sags/swells due to the lack of energy storage devices. PV-fed DVR is used to improve the PQ of grid-connected wind farms from the grid-side disturbances where the PV is mainly used as the energy source for the DVR [21]. In this case, since the PV acts as the DVR energy source, during night time, if any deep power fluctuation happens, the proposed DVR mitigation capability will be low due to its low energy source. Research was conducted to improve the power quality of off-grid hybrid energy sources [22] and conventional grid line energy source [28,29] using DVR. PQ enhancement of grid-connected PV systems using PV-integrated self-supported DVR was conducted [30].

There are different topologies and control strategies of DVR in consideration with performance and cost aspects [25]. The topologies of the DVR could be categorized as with energy storage or without energy storage based on the energy storage perspective [29]. Considering the DVR connection and the energy storage aspect, the topology can be categorized into four types, such as without energy storage supply side connected, without energy storage load side connected, self-charging (capacitor supported), and with external energy storage [20,25,29]. The detection, reference generation, voltage, and current control and modulation aspects of the DVR different controlling schemes are presented in [16,25]. Detection and reference generation are the main parts of the DVR control system [31]. Voltage sag/swell detection is done by measuring the grid voltage and analyzed so that based on sag/swell detection method, the voltage disturbance can be recognized [32]. There are different detection methods such as RMS measurement, dq0 component measurement, wavelet transform, phasor parameter estimation using Kalman filters [25,32]. Among these, dq0 component measurement-based synchronous rotating frame (SRF) control technique is a more popular technique due to its prompt response and simple implementation [25,33]. Generation of reference signal of series-injected voltage will be determined based on the type of energy storage device, its active power supporting capability, and sensitivity of load to voltage disturbances [15,25,32]. Based on this, four basic voltage compensation methods are commonly used such as pre-fault, in-phase, energy optimized, and hybrid compensation methods [25,32]. The only possible way to mitigate the phase jump is to restore the load voltage to the pre-fault value which is addressed by only pre-fault compensation [15,25,28,32].

In this paper, the application of the BES-based DVR to enhance the voltage fluctuation of a grid-connected PV power system is investigated in which the DVR is connected in series between the grid distribution line and the sensitive load. In this study, the proposed BES-based DVR operational time is considered to be high. This is due to the high intermittent scenario of the PV system in addition to any grid fault conditions which all cause voltage fluctuation. This makes the proposed DVR more economical. The output voltage of the DVR is added to the grid distribution voltage instantaneously to be kept a constant voltage at the load during under grid fault condition, during over and under voltage conditions of the PV system, as well as in normal condition. Hence, the grid voltage disturbances have no direct effect on the sensitive load. Therefore, the proposed method is able to eliminate the effect of grid voltage disturbance on sensitive loads. The control algorithm of the DVR system is proposed to overcome voltage sag and swell conditions at the point of common coupling (PCC) so that the sensitive load feeds by a constant voltage. A combination of RMS and dq0 component measurement methods is used for the detection and pre-fault compensation used for reference generation. In addition, a control scheme for the control of the PV system, in which the PV system is integrated with the low voltage (LV) grid side, is designed. The validity of the proposed control algorithm is demonstrated by using the PSCAD simulation. The overall system configuration is presented in Section 2 and the control and compensation strategy is illustrated in Section 3. In Sections 4 and 5, the simulation and results discussion and the conclusion are presented, respectively.

2. System Configuration

Electrical power is generated by a PV system through the conversion of sunlight irradiation using the PV cells which are semiconductor diodes. As the sunlight reaches the PV cell surface, charge carriers are generated from the cells and the electric current produced flows through the short circuit [34,35]. The common PV cell model is presented in Figure 1a which comprises a diode connected to a series and parallel resistance, Rp and Rs, respectively [35].

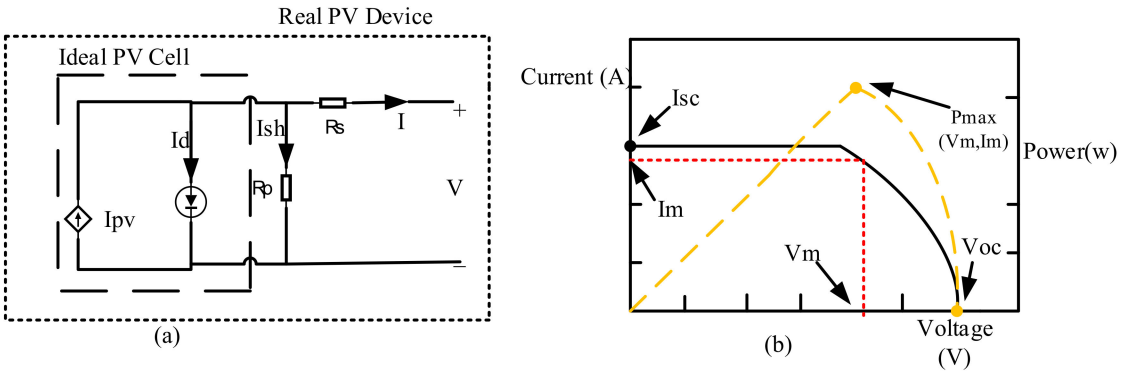

Figure 1. PV cells power circuit and curve: (**a**) PV cell model; (**b**) V-I characteristics with MPPT.

The fast depletion of conventional energy resources, global warming and environmental pollution, technological advancements, and a gradual cost minimization have made RES, such as PV and wind, preferable sources of electric power generation [30,36,37]. The power generated by a PV source is DC and it requires a DC–AC conversion system for grid-integrated operation. DC–DC boost converter, DC–AC converter or VSC, filter, and grid coupling transformer are the main components of the grid-integrated PV system [30] which is illustrated in the proposed scheme in Figure 2 and Figure 5. The PV array is operated at a maximum power point tracking (MPPT) and the converter is synchronized to the grid. As shown in Figure 1b, the maximum output power Pmax of the PV system is described in Equation (1) which is found by the product of maximum current Im and maximum voltage V_m. However, it is rather convenient to use open circuit voltage Voc and short circuit current Isc to estimate the maximum power of cells. To do this, the fill factor (FF) is used which is the fraction of the maximum power that is generated by PV cells to the product of Voc and Isc as expressed in Equation (2) [34]. Voc and Isc will be calculated using Equations (3) and (4) so that the output power of the PV cell Ppv at any time would be found by using Equation (5) where part of the parameters are obtained mainly from the manufacturer data sheets [5].

$$P_{max} = V_{oc} I_{sc} FF \tag{1}$$

$$FF = \frac{V_m I_m}{V_{oc} I_{sc}} \tag{2}$$

$$V_{oc} = V_{oc}^{*} + \beta_v (T - 25) \tag{3}$$

where V_{oc}^{*}, β_v, and T are the V_{oc} of the PV cells under standard test conditions, the PV cells' temperature coefficient referent to V_{oc}, and the cell temperature, respectively.

$$I_{sc} = \frac{G}{G_N} (I_{sc}^{*} + \beta_i (T - 25)) \tag{4}$$

G and G_N are the incident solar irradiance and the incident solar irradiance under standard test conditions, respectively. I_{sc}^{*} and β_i are the PV cells' I_{sc} under standard test conditions and the temperature coefficient of PV cells referent to I_{sc}, respectively.

$$P_{pv} = P_{STC} \frac{G}{G_n} (1 - \gamma (T - 25)) \tag{5}$$

where P_{STC} and γ are the PV cells' maximum power under standard test conditions and maximum power temperature coefficient, respectively.

$$T = T_{amb} + \frac{G}{G_{NOCT}} (T_{c,NOCT} - T_{NOCT}) \tag{6}$$

where T_{amb}, G_{NOCT}, $T_{c,NOCT}$, and T_{NOCT} are the environmental temperature, incident solar irradiance at nominal operating cell temperature, the nominal operating cell temperature provided by the manufacturer, and nominal operating cell temperature, respectively.

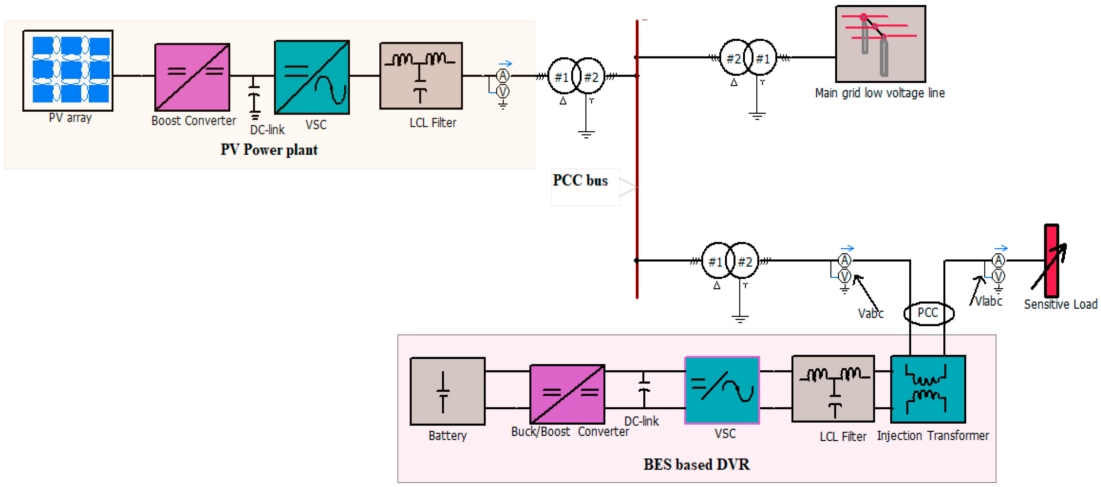

Figure 2. Grid-integrated PV power system with BES-based DVR.

As it is illustrated in Figure 2, the grid-connected PV power system supplies power for a sensitive load and to serve this load with a stable power supply, BES-based DVR is connected in series with the system. In case of fault conditions and PV intermittency, the proposed DVR will operate to protect the load from being damaged and phase-out. As it is shown in Figure 5, the output of a DC–DC boost converter is connected to the DC link capacitor of the VSC. The output voltage generated by the DC–DC boost converter is to be kept along with the average DC input voltage. As described in Figure 2, the PCC bus is the bus where PV power generation and LV grid are connected, whereas PCC is the point where the BES-based DVR is connected to the output terminals of the PCC bus and the sensitive load through its coupling or injection transformer. The main parameters of the grid-connected PV system and the load are presented in Table 1.

Table 1. Grid-integrated PV system parameter specifications.

Parameter	Value
PV transformer	1 kV/6 kV
LV grid transformer	11 kV/6 kV
PCC bus base voltage	6 kV
Distribution transformer	6 kV/0.38 kV
Load	0.2 MW + 0.2 MVAr

A DVR is used to restore the load-side voltage in case of any voltage fluctuation by injecting a voltage of required magnitude and frequency based on the adequate active power capacity. Based on the availability of adequate energy source, the DVR can exchange both active and reactive power at the PCC to compensate the voltage magnitude and phase of sensitive load which is caused by fluctuation. The injected power is a function of the voltage injected and the sensitive load current [17]. As shown in Figure 2 and Figure 7, the DVR has its own BES to have adequate active power capacity and this BES-based DVR has mainly six components such as: battery, buck/boost converter, DC link capacitor (C_{dc}), VSC, LCL filter, and injection transformer. The proper integration and control of these components will result in effective operation of the DVR. The battery charges and discharges based on its capacity, which is measured by its state of charge (SOC). Here, the LCL ripple filters which are placed at the terminals of VSC in both PV generation and BES-based DVR are used for absorbing

switching ripples which are produced by the VSC. The design of the LCL filter's parameters is mainly based on its capability to eliminate the most low- and high-order harmonics of the output voltage waveform. The resonant frequency (f_{res}) attenuates the harmonics generated by the sinusoidal pulse width modulation (SPWM) of the inverter, which occurs near the switching frequency (f_{sw}) which is 5040 Hz. The f_{res} is formulated based on Equation (8), which is dependent on the filter capacitance and filter inductance and obeys the condition expressed in Equation (7) [38–40]. Based on this, the filter inductance was chosen to be 100 uH and the capacitor value should be chosen so that the resonant frequency is less than half of the switching frequency [39,40]. Accordingly, a filter capacitance of 55 mF was chosen to avoid any harmonics with the f_{res} value of around 68 Hz, which is less than half of the f_{sw} which is 2520 Hz. During normal power generation of the PV system, the generated power is fed to the grid in unity power factor mode of operation. However, if the PV power faced intermittency or fault exists at any point upstream of the PCC, then the BES-based DVR operates to protect the sensitive load by stunning the fluctuation. The DVR restores voltage only downstream from the PCC and the compensation is carried phase by phase. The parameters of the proposed BES-based DVR are described in Table 2.

$$f_g \leq f_{res} \leq \frac{f_{sw}}{2} \tag{7}$$

where f_g is the grid frequency, which is 60 Hz.

$$f_{res} = \frac{1}{2\pi\sqrt{LC}} \tag{8}$$

Table 2. BES-based DVR parameter specifications.

Parameter	Value
Filter inductance	0.1 mH
Filter capacitance	55 mF
DC link capacitance	55 mF
DC link rated voltage	550 V
BES capacity	300 Ah
Battery nominal voltage	0.5 kV
Injection transformer rating	0.38 kV/0.38 kV

3. Control Technique and Strategy

Figure 2 depicts the schematic of the proposed system which consists of PV system, grid system, BES-based DVR, and nonlinear load or sensitive load. As depicted in Figure 2, the proposed DVR has a battery system as its external energy storage, which is one of the DVR topology as shown in Figure 3. The different compensation strategies of the DVR are also presented in Figure 4. Figures 5 and 6 illustrate the detailed block diagram of the PV system and its DC-DC converter controlling block diagram respectively. The proposed BES based DVR detailed block diagram is also illustrated in Figure 7. The variable RLC load is used to comprehend a sensitive load. An extensive simulation work is carried out using PSCAD under possible dynamic circumstances, considering the load as sensitive. The control system mainly consists of four subdivisions: the PV system DC–DC boost converter control, the BES DC–DC buck/boost converter control, the PV system VSC control, and the BES-based DVR VSC control as depicted in Figures 6 and 8–10, respectively.

There are different multilevel modulation methods which have been developed for converters and the most commonly used can be classified into three types: (1) carrier-based sinusoidal modulation (SPWM), which includes phase-shifted PWM and phase disposition PWM; (2) space vector modulation (SVPWM); and (3) nearest-level modulation (NLPWM) [41–45]. The SVPWM works with line-to-line voltages which deals simultaneously with all phases, while the other two methods are phase-voltage modulation techniques. The obstacle for applying SVM to multilevel converters is the difficulty caused by the largely increased number of switching states and switching sequences that accompany the higher

number of levels. For a large number of converter levels, NLPWM may be preferable, which directly computes the switching states and duty cycles for each phase of the converter by avoiding triangular waves which are used for SPWM [43]. By selecting proper common-mode voltage injections, SPWM can be functionally equivalent to SVPWM and more specifically, for two-level three-phase converters and lower level converter cases, there are no comparative differences with them [43,45]. Due to this, for all control systems, the SPWM technique is applied in this study. A double loop control is implemented for the two-level three-phase inverters for effective dynamic control of the PV system and the BES-based DVR. The inner loop is used to generate the reference voltages by controlling the output current of the inverter and the outer loop is used to generate the reference currents by controlling the DC voltage.

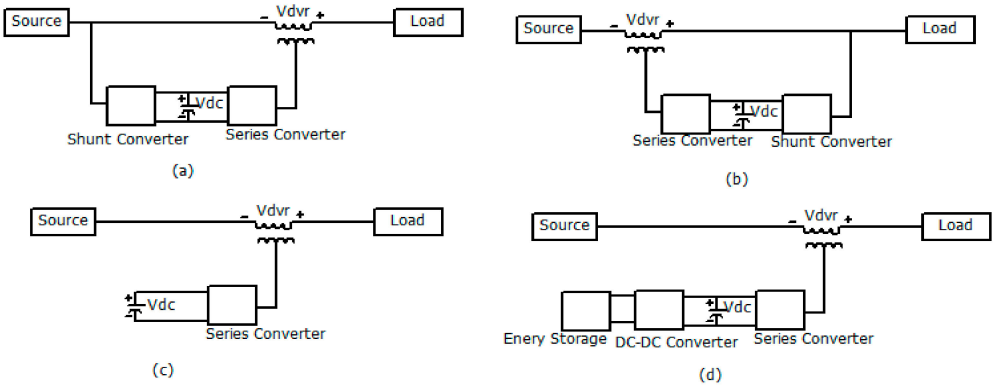

Figure 3. Typical topologies of DVRs: (**a**) without energy storage supply side connected DVR; (**b**) without energy storage load side connected DVR; (**c**) self-charging (capacitor supported) DVR; (**d**) with external energy storage DVR.

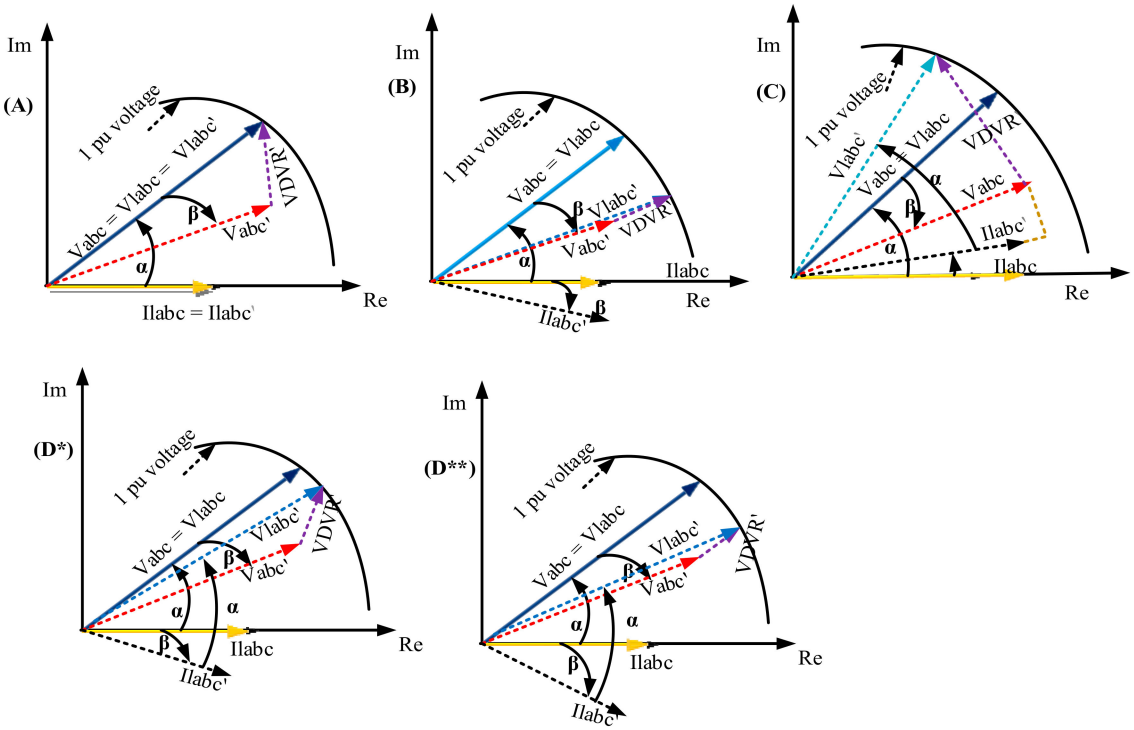

Figure 4. DVR voltage compensation strategies: (**A**) pre-fault; (**B**) in-phase; (**C**) energy optimized; (**D***,**D****) pre-fault and in-phase combination.

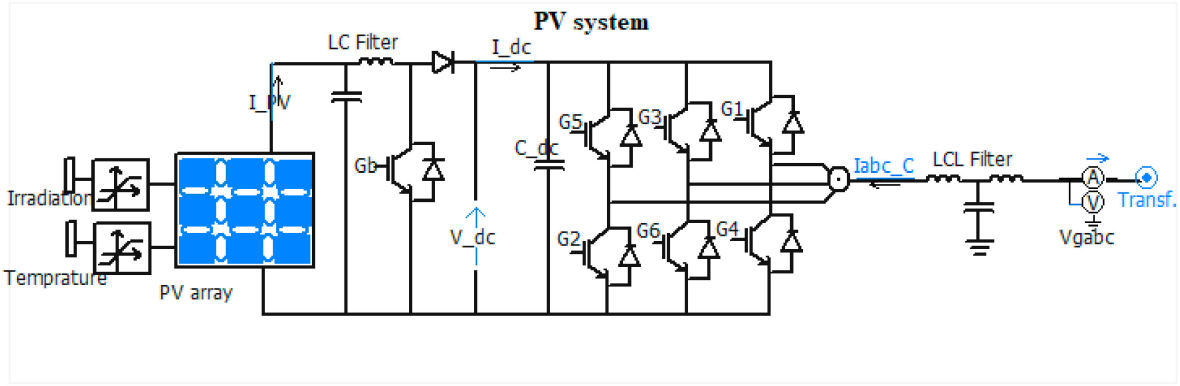

Figure 5. Detailed block diagram of PV system.

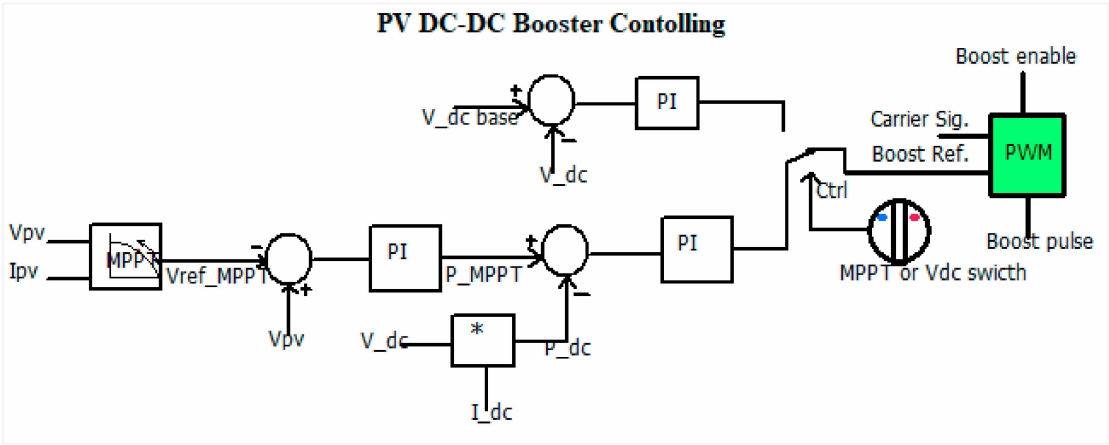

Figure 6. PV DC–DC boost converter controlling diagram.

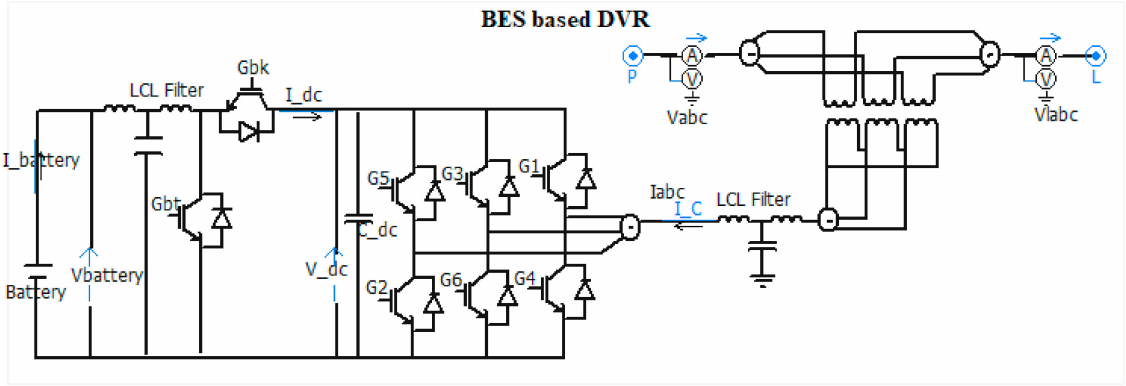

Figure 7. Detailed block diagram of BES-based DVR.

Based on the PV-VSC energy demand, the controlling of the boost converter of a PV system can operate in two modes [41], which are the MPPT and DC voltage control modes as shown in Figure 6. The two control modes can be chosen alternatively by a switch and the main difference between the two modes is the priority of the VSC to supply active or reactive power. The MPPT technique is used to harvest maximum power from the PV array based on Equation (1) when the PV-VSC priority is active power, whereas the DC voltage control mode is used to maintain the DC voltage so that the PV-VSC will control the active power of the DC link and the reactive power is its priority.

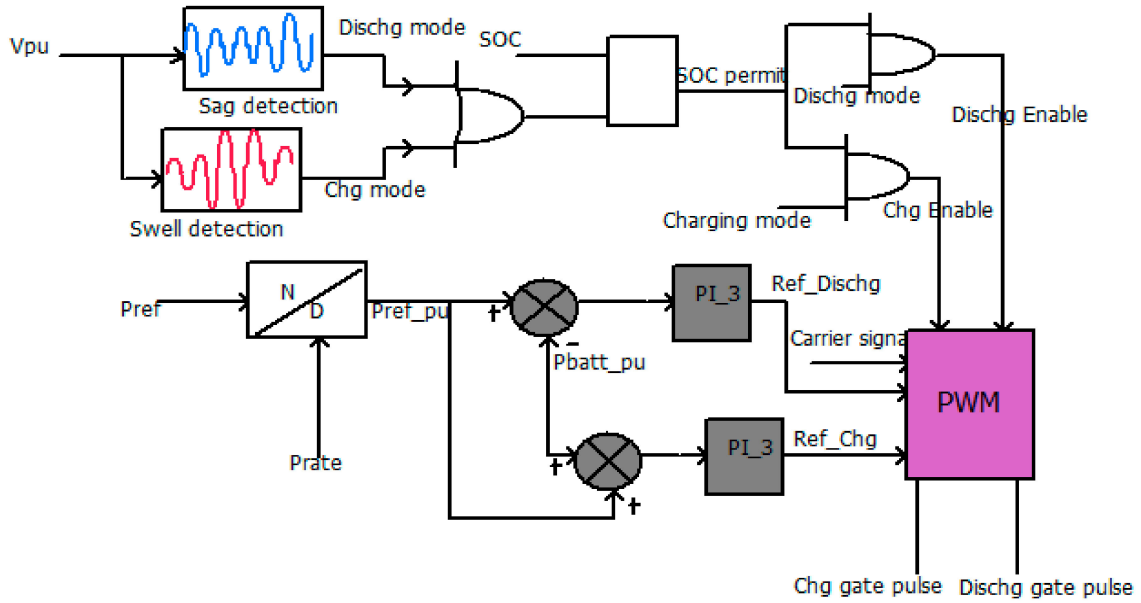

Figure 8. BES buck/boost converter controlling diagram.

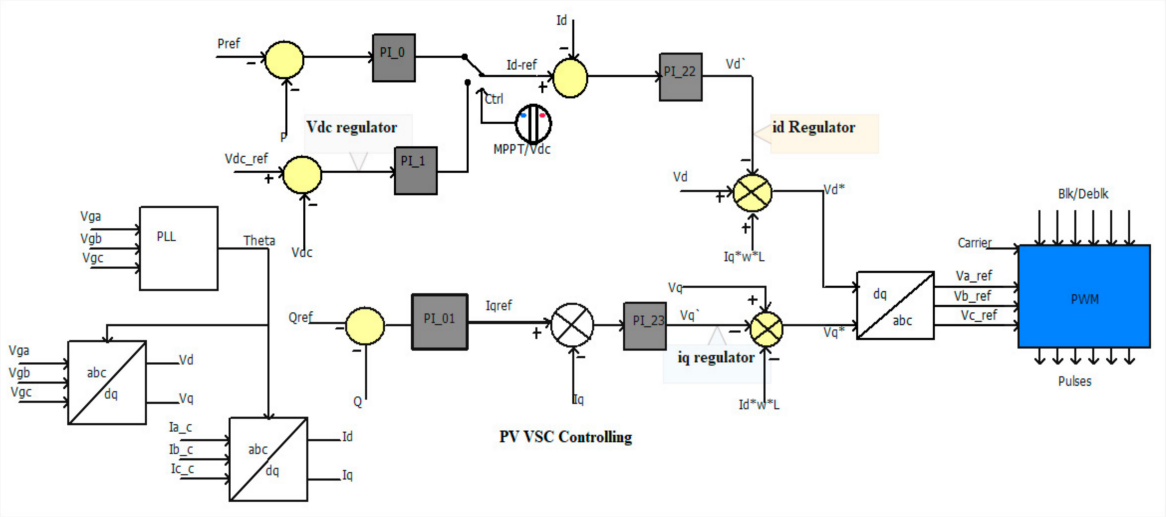

Figure 9. PV system VSC controlling diagram.

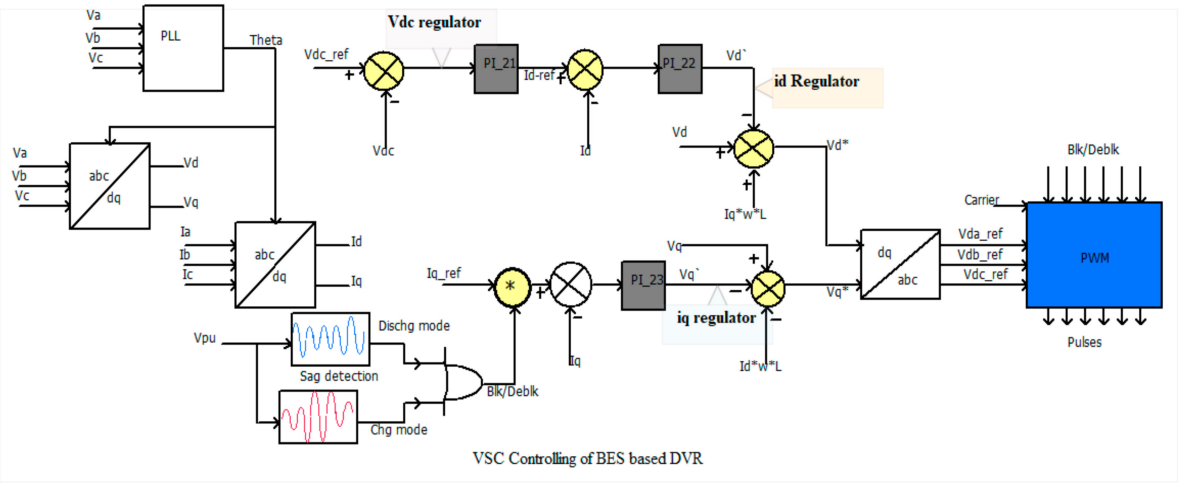

Figure 10. VSC controlling of the BES-based DVR.

The PV system VSC controlling is done using vector-based SRF technique so that reference voltages are generated using instantaneous values of active and reactive voltages and currents. The V_{dq0} component of the three-phase grid voltage at the terminal of the PV system is formulated using park transformation as shown in Equation (9) and the reference voltage is obtained using the inverse park transformation as described in Equation (10). Finally, the reference grid voltage V_{ref} is compared with the triangular carrier signal using SPWM block [12] as shown in Figure 9.

$$\begin{bmatrix} V_d \\ V_q \\ V_0 \end{bmatrix} = \sqrt{\frac{2}{3}} \begin{bmatrix} \sin \varnothing t & \sin\left(\varnothing t - \frac{2\pi}{3}\right) & \sin\left(\varnothing t + \frac{2\pi}{3}\right) \\ \cos \varnothing t & \cos\left(\varnothing t - \frac{2\pi}{3}\right) & \cos\left(\varnothing t + \frac{2\pi}{3}\right) \\ \frac{1}{\sqrt{2}} & \frac{1}{\sqrt{2}} & \frac{1}{\sqrt{2}} \end{bmatrix} \begin{bmatrix} V_{ga} \\ V_{gb} \\ V_{gc} \end{bmatrix} \tag{9}$$

where $\varnothing t$ denotes the transformation angle and V_g represents the grid voltage.

$$\begin{bmatrix} V_{a\_ref} \\ V_{b\_ref} \\ V_{c\_ref} \end{bmatrix} = \sqrt{\frac{2}{3}} \begin{bmatrix} \sin \varnothing t & \cos \varnothing t & \frac{1}{\sqrt{2}} \\ \sin\left(\varnothing t - \frac{2\pi}{3}\right) & \cos\left(\varnothing t - \frac{2\pi}{3}\right) & \frac{1}{\sqrt{2}} \\ \sin\left(\varnothing t + \frac{2\pi}{3}\right) & \cos\left(\varnothing t + \frac{2\pi}{3}\right) & \frac{1}{\sqrt{2}} \end{bmatrix} \begin{bmatrix} V_d \\ V_q \\ V_0 \end{bmatrix} \tag{10}$$

As illustrated in Figure 9, the controlling of PV-VSC is implemented using the SRF transformation. The three-phase voltage and current at the terminal of PV-VSC transform to their respective dq0 component. The voltage vector V_d is affiliated with the direct-axis and V_q is with the quadrature axis. The DC link capacitor voltage V_{dc} is regulated by the power balance at the DC link capacitor by controlling direct axis component of current I_d, whereas the quadrature axis current I_q is used to regulate the reactive power. The MPPT implemented with the PV panels ensures maximum available PV power to flow into the DC link and later to the grid [42]. As shown in Figure 9, the difference of the reference reactive power Q_{ref} and actual reactive power Q is processed through the proportional integral (PI) controller and gives the quadrature reference current I_{qref}. To regulate the quadrature current I_q, the difference of I_{qref} and actual I_q is processed through another PI. On the other hand, the reference direct current I_{dref} is produced either from the difference of the reference DC link voltage V_{dc_ref} and measured DC link voltage V_{dc} or the difference of the actual PV power P and reference PV power P_{ref} and processed through a PI controller using MPPT or V_{dc} selection switch. Through these processes, the reference direct component voltage V_{d*} and quadrature component voltage V_{q*} are processed so that, using the inverse park transformation, the three phase reference voltages V_{a_ref*}, $V_{b_ref*}$and V_{c_ref*} will be formulated. These reference voltages are compared with carrier signal using the SPWM technique to generate pulses for each respective insulated-gate bipolar transistor (IGBT) switches $G_1 - G_6$. Finally, the high-frequency component and DC offset voltages at the terminal of PV-VSC is filtered by LCL low pass filter and integrated into the grid.

Disturbance detection and reference generation are the main parts of the DVR control system. There are different detection methods such as RMS measurement, dq0 component measurement, wavelet transform, and phasor parameter estimation using Kalman filters [25,32]. Among these, vector-based SRF dq0 component measurement control technique is a more popular technique due to its prompt response and simple implementation [25,33]. Generation of reference voltage will be determined based on the type of energy storage device, its active power supporting capability, and voltage disturbances sensitivity of the load [15,25,32]. Based on the reference generation, the DVR voltage compensation strategies can be classified as pre-fault, in-phase, energy optimized, and a hybrid compensation (combination of pre-fault and in-phase compensation) [17,25,32] as depicted in Figure 4. The pre-fault compensation restores the voltage to its pre-fault value both in magnitude and phase angle, whereas phase compensation restores voltage only in phase with the voltage during fault which means it only restores the magnitude to pre-fault value but not the phase angle. The energy optimized compensation tries to reduce the real power injection so it may restore phase angles only partially. The hybrid compensation has the features of both pre-fault and in-phase compensation which operates

for some time in pre-fault compensation and other times shifts to in-phase compensation. For sensitive loads, restoration of both magnitude and phase angle is necessary, so pre-fault compensation is used in this study due to its capability to restore both.

In the proposed control scheme of the BES-based DVR, two control strategies are used where one is for the buck/boost converter and the other is for the VSC as depicted in Figures 8 and 10, respectively. For the buck/boost converter controlling, the RMS voltage is measured on the upstream side of the PCC and fed as input to permit the battery to charge and discharge based on its SOC value as shown in Figures 7 and 8. The boost switch (G_{bt}) and buck switch (G_{bk}) are used to discharge and charge the battery, respectively. Based on the reference power (P_{ref}) and rated battery power (P_{rate}), the reference charging and discharging signals are generated using separate PI controllers. In the other case, using the RMS measured voltage (V_{pu}) and SOC value of the battery, the SOC permits blocking and deblocking of G_{bt} and G_{bk} switches. To protect the battery from overcharging and discharging, charging of the battery is permitted if and only if the SOC value is less than 100% and discharging of the battery is permitted if and only if the SOC value is in the interval of 5–100%.

Figure 10 shows the proposed control block diagram of the VSC of the DVR which developed using RMS voltage measurement and dq0 component measurement detection techniques and pre-fault compensation strategy. Here, V_{abc} (V_a, V_b, V_c) and I_{abc} (I_a, I_b, I_c) are the voltage at the upstream side of PCC and the current flowing at the terminal of the DVR VSC, respectively. Based on the park transformation, the three-phase abc voltage and current components change to dq0 components and the phase angle is taken from phase locked loop (PLL) which is used to lock the phase angle of the system during normal condition before the fault. I_d is used to regulate V_{dc} and I_q is used to regulate the reactive power. To regulate V_{dc}, the difference between V_{dc}_ref and measured V_{dc} is processed by the PI controller and generates I_{d_ref}. Then after, I_d and I_{d_ref} difference is processed through another PI controller to regulate I_d. On the other hand, by detecting the sag/swell condition using V_{pu} value, its output value Blk/Deblk is multiplied with I_{q_ref} and the difference with I_q is processed through the PI controller to regulate I_q component. Finally, the reference direct axis (V_d*) and quadrature axis (V_q*) voltages are processed so that using the inverse park transformation, the reference voltages (V_{da_ref}, V_{db_ref}, V_{dc_ref}) are processed. These reference voltages are compared with the triangular carrier signal using the SPWM block to generate pulses for each respective IGBT switches $G_1 - G_6$. The terminal voltage of VSC will be transmitted to the LCL filter to eliminate harmonics and DC offsets and finally the DVR will inject this appropriate voltage to the sensitive load though the injection transformer.

4. Simulation Results and Discussion

A fault was applied at the PCC bus by varying the fault resistance to form different sag depths for both symmetrical and asymmetrical scenarios. Figures 11 and 12 illustrate a single line to ground (LG) fault with different fault resistance which is 2 ohms and 4 ohms, respectively. Due to this, the sag depth and the DVR compensation voltage are higher in Figure 11 compared to Figure 12. Even though the fault is LG, due to the delta-wye connection of the distribution transformer and severity of the fault, the impact of the fault affects the other phase also and makes double phase sag with different sag depth. Figure 11a shows the load voltage during LG fault at phase a produces a deep sag for the particular phase a, and a slight sag for phase c. The phase a sag is more than 33% and in phase c, it is around 20%. Since the voltage variation is more than 10% from the nominal value, based on the control techniques applied, the BES-based DVR operates and compensates the voltage sag as it is seen in Figure 11b,c. In Figure 12a, LG fault is applied at phase a with higher fault resistance value compared to Figure 11 and due to this, the fault affects only the faulted line.

As described in Figure 13a, all the three-phase load voltages are sagged more than 40% from the nominal value due to a three-phase ground fault (LLLG) at the PCC bus with a fault resistance of 2.5 ohms.

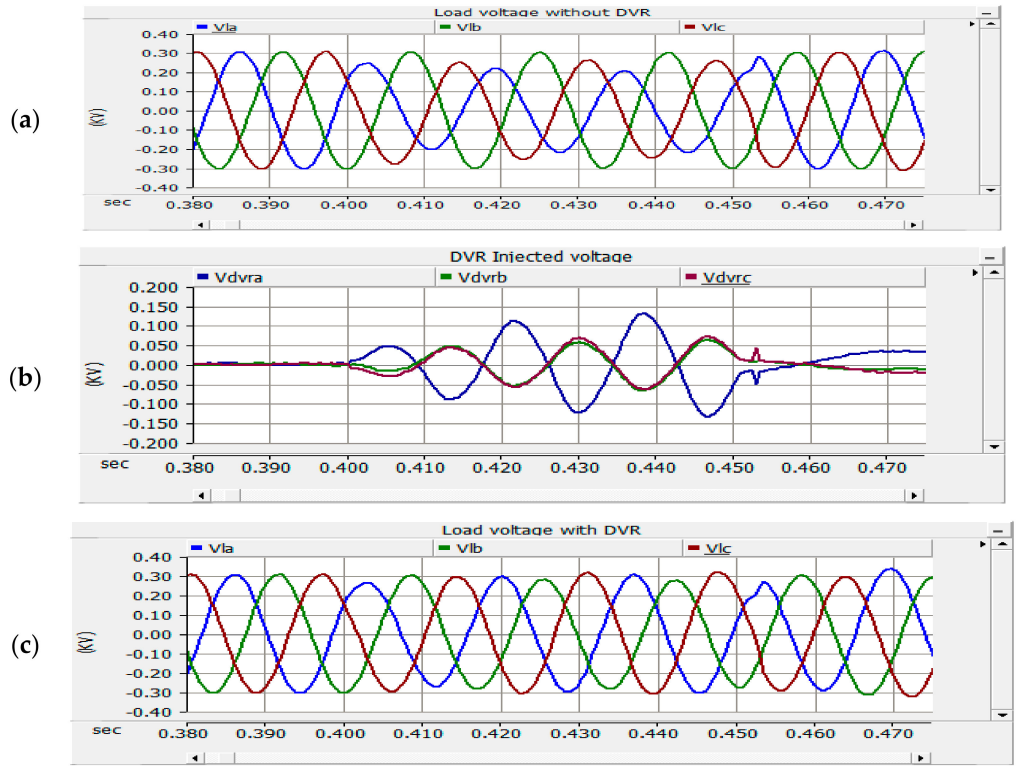

Figure 11. 33% double phase voltage sag and compensation: (**a**) load voltage without DVR; (**b**) DVR injected voltage; (**c**) load voltage with DVR.

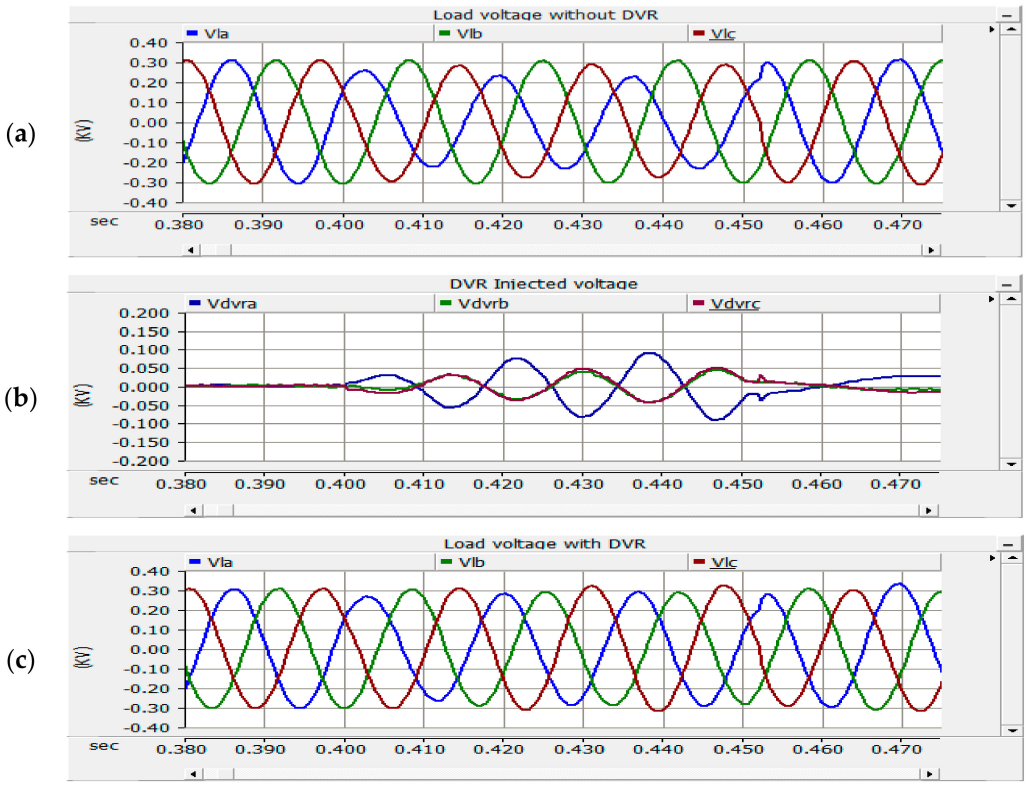

Figure 12. 30% single phase voltage sag and compensation: (**a**) load voltage without DVR; (**b**) DVR injected voltage; (**c**) load voltage with DVR.

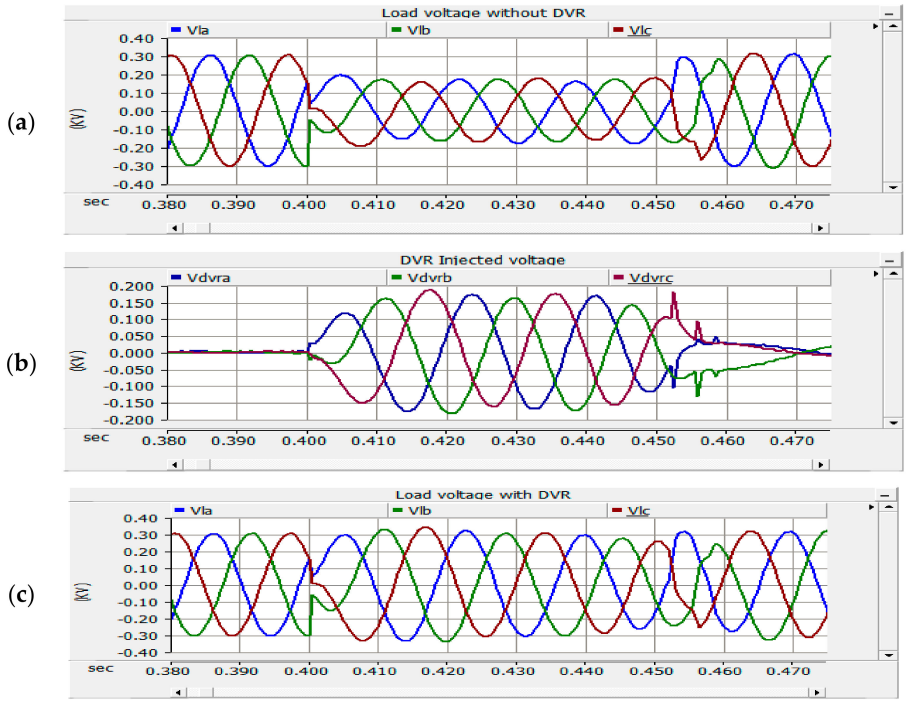

Figure 13. 40% symmetrical phase voltage sag and compensation: (**a**) load voltage without DVR; (**b**) DVR injected voltage; (**c**) load voltage with DVR.

By operating the BES-based DVR, the sagged voltage is compensated as shown in Figure 13b,c. On the other hand, the LLLG fault happened at the PCC bus with fault resistance of 4 ohms and a more than 30% symmetrical voltage sag happened as shown in Figure 14a. By using the BES-based DVR, it is restored to normal as presented in Figure 14b,c.

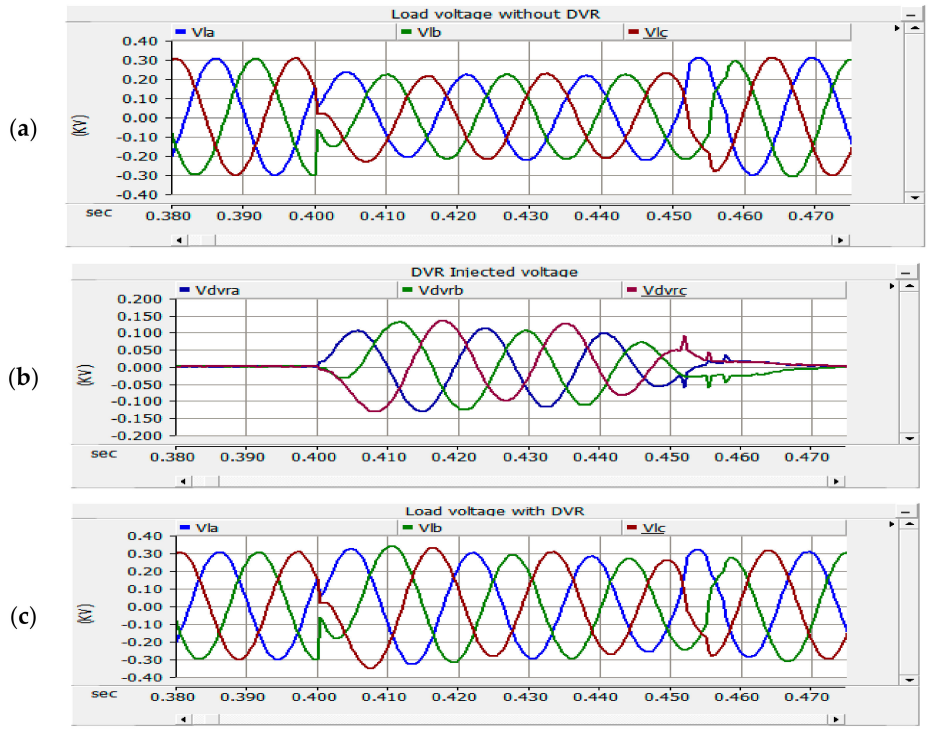

Figure 14. 40% symmetrical phase voltage sag and compensation: (**a**) load voltage without DVR; (**b**) DVR injected voltage; (**c**) load voltage with DVR.

During PV system intermittence situations also, voltage fluctuation will happen at the PCC bus so that the sensitive load will face PQ problems. To overcome this problem, the proposed BES-based DVR will operate in the same way as the fault cases simulated above. Due to this, the probability of operation of the DVR will be high during night time and cloud conditions since the PV system will not work with its nominal voltage. This makes the proposed DVR more economical as its operation increases.

5. Conclusions

The advancement of power electronic-based devices increases the issue of PQ due to its sensitivity to power fluctuation. When sensitive loads get power from grid-integrated PV/wind power systems, their vulnerability will increase due to the intermittent nature of PV/wind power sources. In this study, the sensitive load gets power from the grid-integrated PV system. The supply voltage for the load could be fluctuated either due to faults in the upstream of the load or due to the source intermittency of the PV system. In this study, a fault is applied at the PCC bus to form voltage fluctuation at the load. The proposed BES-based DVR operates when voltage deviation is greater than 10% of nominal voltage. The PV system is integrated with the grid system with a proper controlling of its boost converter and VSC. Based on the priority of active power or reactive power support of the system, these converters can be controlled by the MPPT mode or DC-link mode. The BES-based DVR operates by proper controlling of buck/boost converter of the battery and VSC of the DVR. The detection and reference generation are the two main controlling techniques of the proposed DVR where a combination of RMS and dq0 measurement is used for detection, and pre-fault compensation is used for reference generation control due to its capability of phase jump and magnitude restoration. The effectiveness of the proposed BES-based DVR is demonstrated for both symmetrical and asymmetrical sag conditions with different sag depths. The proposed system also could be very useful for microgrid systems which provide power to sensitive loads.

Author Contributions: This research article was done with supervision, validation, writing—review and editing and visualization of C.-C.K. and conceptualization, methodology, formal analysis, software, investigation, writing—original draft preparation was done by E.M.M. All authors have read and agreed to the published version of the manuscript.

Funding: This research received no external funding.

Conflicts of Interest: The authors declare no conflict of interest.

References

1. Pérez, E.; Beltran, H.; Aparicio, N.; Rodríguez, P.; Member, S. Predictive Power Control for PV Plants with Energy Storage. *IEEE Trans. Sustain. Energy* **2013**, *4*, 482–490. [CrossRef]
2. IRENA. *Future of Solar Photovoltaic: Deployment, Investment, Technology, Grid Integration and Socio-Economic Aspects (A Global Energy Transformation: Paper)*; International Renewable Energy Agency: Abu Dhabi, UAE, 2019.
3. IRENA. *Renewable Energy Market Analysis*; GCC. IRENA: Abu Dhabi, UAE, 2019.
4. U.S. Energy Information Administrat. *International Energy Outlook 2019*; U.S. Energy Information Administrat: Washington, DC, USA, 2019.
5. Riffonneau, Y.; Bacha, S.; Barruel, F.; Ploix, S. Optimal Power Flow Management for Grid Connected PV Systems With Batteries. *IEEE Trans. Sustain. Energy* **2011**, *2*, 309–320. [CrossRef]
6. Wang, G.; Ciobotaru, M.; Agelidis, V.G. Power Smoothing of Large Solar PV Plant Using. *IEEE Trans. Sustain. Energy* **2014**, *5*, 834–842. [CrossRef]
7. Hasanien, H.M.; Member, S. An Adaptive Control Strategy for Low Voltage Ride Through Capability Enhancement of Grid-Connected Photovoltaic Power Plants. *IEEE Trans. Power Syst.* **2016**, *31*, 3230–3237. [CrossRef]
8. Liu, Q.; Li, Y.; Luo, L.; Peng, Y.; Cao, Y. Power Quality Management of PV Power Plant With. *IEEE Trans. Power Deliv.* **2019**, *34*, 941–949. [CrossRef]
9. Sanjari, M.J.; Gooi, H.; Member, S.; Nair, N.C.; Member, S. Power Generation Forecast of Hybrid PV—Wind System. *IEEE Trans. Sustain. Energy* **2020**, *11*, 703–712. [CrossRef]

10. Krama, A.; Zellouma, L.; Rabhi, B.; Refaat, S.S. Real-Time Implementation of High Performance Control Scheme for Grid-Tied PV System for Power Quality Enhancement Based on MPPC-SVM. *Energies* **2018**, *11*, 3516. [CrossRef]
11. Muthuvel, K.; Vijayakumar, M. Solar PV Sustained Quasi Z-Source Network-Based Unified Power Quality Conditioner for Enhancement of Power Quality. *Energies* **2020**, *13*, 2657. [CrossRef]
12. Ray, P.K.; Member, S.; Das, S.R.; Mohanty, A. Fuzzy-Controller-Designed-PV-Based Custom Power Device for Power Quality Enhancement. *IEEE Trans. Enrgy Convers.* **2019**, *34*, 405–414. [CrossRef]
13. Gautam, P.; Piya, P.; Karki, R. Development and Integration of Momentary Event Models in Active Distribution System. *IEEE Trans. Power Syst.* **2020**, *35*, 3236–3246. [CrossRef]
14. Ray, P.K.; Mohanty, A.; Panigrahi, T. Power quality analysis in solar PV integrated microgrid using independent component analysis and support vector machine. *Opt. Int. J. Light Electron. Opt.* **2019**, *180*, 691–698. [CrossRef]
15. Rauf, A.M.; Khadkikar, V. An Enhanced Voltage Sag Compensation Scheme for Dynamic Voltage Restorer. *IEEE Trans. Ind. Electron.* **2015**, *62*, 2683–2692. [CrossRef]
16. Chishti, F.; Murshid, S.; Singh, B. Unbiased Circular Leakage Centered Adaptive Filtering Control For Power Quality Improvement of Wind—Solar PV Energy Conversion System. *IEEE Trans. Sustain. Energy* **2020**, *11*, 1347–1357. [CrossRef]
17. Zhang, Y. Modeling of FACTS Devices for Voltage Sag Mitigation Studies in Large Power Systems. *IEEE Trans. Power Deliv.* **2010**, *25*, 3044–3052. [CrossRef]
18. Kumar, N.; Singh, B. Framework of Gradient Descent Least Squares Regression-Based NN Structure for Power Quality Improvement in PV-Integrated Low-Voltage Weak Grid System. *IEEE Trans. Ind. Electron.* **2019**, *66*, 9724–9733. [CrossRef]
19. Jamil, E.; Hameed, S.; Jamil, B. Power quality improvement of distribution system with photovoltaic and permanent magnet synchronous generator based renewable energy farm using static synchronous compensator. *Sustain. Energy Technol. Assess.* **2019**, *35*, 98–116. [CrossRef]
20. Molla, E.M.; Liu, C.; Kuo, C. Power quality improvement using microsystem technology for wind power plant. *Microsyst. Technol.* **2020**, *26*, 1799–1811. [CrossRef]
21. Priyavarthini, S.; Kathiresan, A.C.; Nagamani, C.; Ilango, S. PV-fed DVR for simultaneous real power injection and sag / swell mitigation in a wind farm. *IET Power Electron.* **2018**, *11*, 2385–2395. [CrossRef]
22. Hassanein, W.S.; Ahmed, M.M.; Osama, M.; Ashmawy, M.G.; Mosaad, M.I. Performance improvement of off-grid hybrid renewable energy system using dynamic voltage restorer. *Alex. Eng. J.* **2020**, *59*, 1567–1581. [CrossRef]
23. Mosaad, M.I.; El-raouf, M.O.A.; Al-ahmar, M.A.; Bendary, F.M. Optimal PI controller of DVR to enhance the performance of hybrid power system feeding a remote area in Egypt. *Sustain. Cities Soc.* **2019**, *47*, 101469. [CrossRef]
24. Sagha, H.; Mokhtari, G.; Arefi, A.; Nourbakhsh, G.; Ledwich, G.; Ghosh, A. A New Approach to Improve PV Power Injection in LV Electrical Systems Using DVR. *IEEE Syst. J.* **2018**, *12*, 3324–3333. [CrossRef]
25. Farhadi-kangarlu, M.; Babaei, E.; Blaabjerg, F. A comprehensive review of dynamic voltage restorers. *Int. J. Electr. Power Energy Syst.* **2017**, *92*, 136–155. [CrossRef]
26. Ibrahim, A.O.; Nguyen, T.H.; Member, S.; Lee, D.; Kim, S. A Fault Ride-Through Technique of DFIG Wind Turbine Systems Using Dynamic Voltage Restorers. *IEEE Trans. Energy Convers.* **2011**, *26*, 871–882. [CrossRef]
27. Agalar, S.; Kaplan, Y.A. Power quality improvement using STS and DVR in wind energy system. *Renew. Energy* **2018**, *118*, 1031–1040. [CrossRef]
28. Zheng, Z.; Xiao, X.; Chen, X.; Huang, C.; Zhao, L.; Li, C. Performance Evaluation of a MW-Class SMES-BES DVR System for Mitigation of Voltage. *IEEE Trans. Ind. Appl.* **2018**, *54*, 3090–3099. [CrossRef]
29. Wang, J.; Member, S.; Xing, Y. A Novel Dual-DC-Port Dynamic Voltage Restorer With Reduced-Rating Integrated DC—DC Converter for Wide-Range Voltage Sag Compensation. *IEEE Trans. Power Electron.* **2019**, *34*, 7437–7449. [CrossRef]
30. Rauf, A.M.; Khadkikar, V. Integrated Photovoltaic and Dynamic Voltage Restorer System Configuration. *IEEE Trans. Sustain. Energy* **2015**, *6*, 400–410. [CrossRef]
31. Molla, E.M.; Kuo, C. Voltage Sag Enhancement of Grid Connected Hybrid PV-Wind Power System Using Battery and SMES Based Dynamic Voltage Restorer. *IEEE Access* **2020**, *8*, 130003–130013. [CrossRef]
32. Sadigh, A.K.; Member, S.; Smedley, K.M. Review of voltage compensation methods in dynamic voltage restorer (DVR). In *IEEE Power and Energy Society General Meeting*; IEEE: New York, NY, USA, 2012; pp. 1–8.

33. Converters, G.V.; Somkun, S.; Chunkag, V. Frame Current Control for Single-Phase. *IEEE Trans. Ind. Electron.* **2016**, *63*, 5425–5436.
34. Carvalho, D.B.; Guardia, E.C.; Lima, J.W.M. Technical-economic analysis of the insertion of PV power into a wind-solar hybrid system. *Sol. Energy* **2019**, *191*, 530–539. [CrossRef]
35. Benali, A. Power Quality Improvement and Low Voltage Ride Through Capability in Hybrid Wind-PV Farms Grid-Connected Using Dynamic Voltage Restorer. *IEEE Access* **2018**, *6*, 68634–68648. [CrossRef]
36. Al-masri, H.M.; Member, S.; Ehsani, M.; Fellow, L. Feasibility Investigation of a Hybrid On-Grid Wind Photovoltaic Retrofitting System. *IEEE Trans. Ind. Appl.* **2016**, *52*, 1979–1988. [CrossRef]
37. Karanayil, B.; Ceballos, S.; Pou, J. Maximum Power Point Controller for Large-Scale Photovoltaic Power Plants Using Central Inverters Under Partial Shading Conditions. *IEEE Trans. Power Electron.* **2019**, *34*, 3098–3109. [CrossRef]
38. Drives, V.V.A.C.M.; Hatua, K.; Jain, A.K.; Member, S. Active Damping of Output LC Filter Resonance for. *IEEE Trans. Ind. Electron.* **2012**, *59*, 334–342.
39. Liserre, M.; Blaabjerg, F.; Hansen, S. Design and Control of an LCL -Filter-Based Three-Phase Active Rectifier. *IEEE Trans.* **2005**, *41*, 1281–1291. [CrossRef]
40. Sa, M.B.; Naouar, M.W.; Belkhodja, I.S.; Monmasson, E. Simple and systematic LCL filter design for three-phase grid-connected power converters. *Math. Comput. Simul.* **2016**, *130*, 181–193.
41. Simple Solar Farm. Available online: https://www.pscad.com/knowledge-base/article/521 (accessed on 21 June 2019).
42. Wandhare, R.G.; Agarwal, V. Novel Stability Enhancing Control Strategy for Centralized PV-Grid Systems for Smart Grid Applications. *IEEE Trans. Smart Grid* **2014**, *5*, 1389–1396. [CrossRef]
43. Deng, Y.; Member, S.; Harley, R.G. Space-Vector Versus Nearest-Level Pulse Width Modulation for Multilevel Converters. *IEEE Trans. Power Electron.* **2015**, *30*, 2962–2974. [CrossRef]
44. Brand, N.; Acobina, C.B.; Maia, A.C.N.; Melo, V.F.M.B. Six-Leg Single-Phase Multilevel Rectifier Inverter: PWM Strategies and Control. *IEEE Trans. Ind. Appl.* **2017**, *53*, 350–361.
45. Iqbal, A.; Moinuddin, S. Comprehensive Relationship Between Carrier-Based PWM and Space Vector PWM in a Five-Phase VSI. *IEEE Trans. Power Electron.* **2009**, *24*, 2379–2390. [CrossRef]